

Theory of magneto-electric photocurrent generated by direct inter-band transitions in semiconductor quantum well

Hai-Zhou Lu,^{1,*} Bin Zhou,² Fu-Chun Zhang,¹ and Shun-Qing Shen^{1,†}

¹*Department of Physics and Center for Theoretical and Computational Physics,
The University of Hong Kong, Pokfulam Road, Hong Kong, China*

²*Department of Physics, Hubei University, Wuhan 430062, China*

(Dated: February 15, 2019)

A linearly polarized light normally incident on a semiconductor quantum well with Rashba spin-orbit coupling may generate pure spin current via direct interband optical transition. An electric photocurrent is induced when an in-plane magnetic field is applied, which has been recently observed in experiments [Dai *et al.*, Phys. Rev. Lett. **104**, 246601 (2010)]. Here we present a systematic theoretical study of this magneto-electric photocurrent effect associated with the interband transition. By employing the density matrix formalism, we calculate the photoexcited carrier density, electric current density, and spin current density. We show that the photoexcited carrier density has an anisotropic distribution in k space, strongly depending on the orientation of the wave vector and the polarization of the light. Our theory explains the observed dependences of the photocurrent on the magnetic field and the polarization of the light. We also show that the ratio of the pure spin photocurrent and the magnetic field induced electric photocurrent is approximately equal to the ratio of the kinetic energy over the Zeeman energy, which enables us to estimate the pure spin photocurrent.

PACS numbers: 42.65.-k, 72.25.Dc, 72.40.+w, 73.63.Hs

I. INTRODUCTION

Optical injection and detection of spin current have recently attracted a lot of interest in the context of non-magnetic semiconductor spintronics.^{1,2} Important progresses made so far include the injection of spin-polarized currents by using the spin galvanic effect³ and the circular photogalvanic effect,⁴ the observation of spin accumulations induced by the spin Hall effect with the help of the Kerr rotation⁵ and the p-n junction light emit diode,⁶ and the inverse spin Hall effect.^{7,8}

Generation and detection of the pure spin current where there is not net charge current is one of the challenging issues in spintronics. Optically, the generation of pure spin photocurrent has been realized by injecting orthogonally polarized one- and two-photon linear lights,^{9–13} or by the incidence of unpolarized or linearly polarized lights into bulk III-V semiconductors and quantum wells with spin-orbit couplings.^{14–19} In the latter case, a linearly polarized light can be decomposed into circularly polarized lights with opposite helicities. Due to the conservation of angular momentum, the circularly polarized lights with opposite helicities excite carriers with opposite spins, which are locked to opposite momenta owing to the spin-orbit coupling. As a result, the photo-injected carriers with opposite spins have opposite velocities, leading to the pure spin photocurrent. One way to observe this underlying pure spin photocurrent is to apply an in-plane magnetic field, which will create an imbalance of spins. The spin imbalance leads to the asymmetry of electron velocities by the spin-orbit coupling and can extract an electric photocurrent from the pure spin photocurrent. The field-induced conversion from pure spin photocurrent to electric photocurrent (also referred to as magneto-gyrotropic photogalvanic effect, MPGE) was systematically studied via the intra-band^{20,21} and inter-subband²² electron heating by THz and microwave radiations, in which spin-dependent scatterings are necessary for the observed charge current.

Very recently, the magnetic field induced electric photocurrent has been observed via direct interband optical transitions.²³ Unlike the intra-band transition, in the direct interband transition the electron momentum is conserved, and the magnetic field induced electric photocurrent is a few orders of magnitude larger than that via the intraband transition. Therefore, it appears to be promising as a simple and practical method to generate and detect the spin current.

In this work, we study theoretically the generation of photocurrent via direct interband transitions excited by shedding a linearly polarized light normally into a semiconductor quantum well. We find that the k -space anisotropy of the carrier density excited by the linear light in the spin-split bands provides a clear microscopic picture for the magnetic field induced electric photocurrent and pure spin photocurrent at zero field. The experimental results, including the polarization angle and magnetic field dependences, can be well described within the picture. Moreover, we propose an approach to estimate the magnitude of the undetectable pure spin photocurrent, which is generated at zero magnetic field by the same linear light, from the observed field-induced electric photocurrent. Part of the results was very briefly reported in Ref. 23.

The paper is organized as follows. In Sec. II, we review key features of the experimentally observed electric photocurrent as a function of magnetic fields and the polarization of the linear light, and present a symmetry argument. In Sec. III, a standard density matrix formalism is applied to the direct interband optical absorption in a two-dimensional quantum well described by the Rashba and Kohn-Luttinger models. In Sec. IV, we introduce microscopic physical picture of the anisotropic photoexcited carrier density in k space. In Sec. V, we will explain the origins of the magnetic field induced electric photocurrent in terms of the anisotropic photoexcited carrier density. In Sec. VI, the estimate of the underlying pure spin photocurrent at zero magnetic field is discussed. Finally, a summary is given in Sec. VII.

II. BRIEF REVIEW OF EXPERIMENT

In this section, we will review the experimental results on the magnetic field induced electric photocurrent generated via direct interband optical transitions by shedding a linearly polarized light normally into an InGaAs/InAlAs quantum well.²³ The experiment setup reported in Ref. 23 is schematically illustrated in Fig. 1.

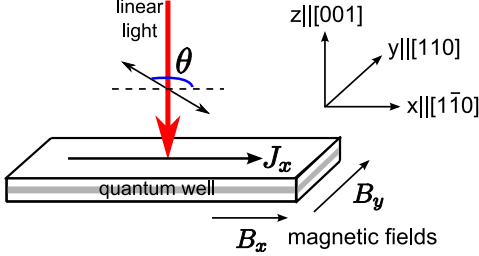


FIG. 1: Schematic illustration of the setup reported in Ref. 23, in which a linearly polarized light (downward arrow) is normally incident into a semiconductor quantum well grown along the [001] direction of zinc-blende materials. θ denotes the light polarization angle with respect to x -axis. The x , y , and z axes are defined along $[1\bar{1}0]$, $[110]$, and $[001]$ crystallographic directions, respectively. B_x (B_y) indicates the parallel (perpendicular) magnetic field with respect to the generated photocurrent J_x .

In the reported experiments, the current measured along x direction as a function of the light polarization and magnetic fields can be summarized as²³

$$J_x = c_0 B_y + c_y B_y \cos 2\theta + c_x B_x \sin 2\theta, \quad (1)$$

where B_x and B_y are the magnetic fields along x and y directions, respectively. θ is the polarization angle of the linearly polarized light with respect to x axis. $c_{0,x,y}$ are constant coefficients. The x and y axes here are defined along $[1\bar{1}0]$ and $[110]$ crystallographic directions of the zinc blende structure, respectively.

The experimental results are consistent with the symmetry argument of the C_{2v} point group.²¹ Inversion-asymmetric zinc blende heterostructures grown along $[001]$ crystallographic direction usually have the C_{2v} point group symmetry. As a result, the electric photocurrent density induced by in-plane magnetic fields can be phenomenologically written as (please refer to Appendix A for details)

$$j_\mu = \sum_\nu (\chi^{\mu\mu\nu\bar{\nu}} B_\mu E_\nu E_{\bar{\nu}} + \chi^{\mu\bar{\mu}\nu\nu} B_{\bar{\mu}} E_\nu E_\nu), \quad (2)$$

where μ, ν run over $\{x, y\}$, and $\bar{\mu}, \bar{\nu} = y$ if $\mu, \nu = x$, and vice versa. χ is a fourth-rank pseudo tensor that relates the electric photocurrent densities to the polarization electric field components (E_x, E_y) $\propto (\cos \theta, \sin \theta)$ of the incident light and magnetic fields (B_x, B_y). One can readily check that Eq. (2) yield the same form as Eq. (1). This symmetry analysis is general for materials and structures with the C_{2v} symmetry, while the specific microscopic picture of optical absorption can cover a wide range of possibilities.

In addition, the invariants of the C_{2v} symmetry requires that when defining $x||[1\bar{1}0]$ and $y||[110]$, the spin-orbit coupling can only be of the Rashba type^{24,25} (please refer to Appendix A for details)

$$H_{\text{SOC}} = \alpha_x \sigma_y k_x - \alpha_y \sigma_x k_y, \quad (3)$$

where $k_{x/y}$ is the wave vector along x (y) axis, the Pauli matrix $\sigma_{x/y}$ depicts the spin along x (y) direction, and $\alpha_{x/y}$ is the Rashba coefficient along x (y) direction. As we know, the current along x direction corresponds to the average shift of momenta of carriers along x direction. According to Eq. (3), k_x couples only to the spin along y directions, thus it can only be shifted by a magnetic field along y direction. Under this argument, the last term of Eq. (1) seems against intuition because it originates from a magnetic field along x direction.

The magnetic field and polarization angle dependences of the electric photocurrent will be explained in the following sections, in terms of the anisotropy of the photoexcited carrier density in \mathbf{k} space. We will see that the three terms in Eq. (1) can be well interpreted by the microscopic picture presented in Fig. 4 (subfigures in boxes).

III. THEORY OF DIRECT INTERBAND OPTICAL EXCITATION

In this section, we provide theoretical study of the experiment in Ref. 23. A quantum well is grown along the $[001]$ crystallographic direction of inversion-asymmetric zinc blende materials. In the quantum well, we assume that two conduction bands and four valence bands are enough to account for the experimental features. The conduction and valence bands are separated by an energy gap Δ . A single-frequency linearly polarized light is incident normally into the quantum well. The frequency of the light ω is larger than the energy gap, therefore the dominant optical absorption mechanism is the direct interband transition. ‘‘Direct’’ means that the wave vector \mathbf{k} of electron keeps unchanged in the transition. The electric measurement is performed along $[1\bar{1}0]$ and $[110]$ crystallographic directions, which are defined as x and y axes, respectively.

A. Hamiltonian

The total Hamiltonian consists of two conduction (H_C) and four valence (H_V) bands and their interaction with the light [$\hat{V}(t)$],

$$H = H_C + H_V + \hat{V}(t), \quad (4)$$

where the lowest conduction subbands are described by a two-dimension free electron gas with the Rashba spin-orbit coupling and in-plane magnetic fields

$$H_C = \frac{\hbar^2}{2m^*} (k_x^2 + k_y^2) + \alpha(\sigma_x k_y - \sigma_y k_x) + \mathbf{h} \cdot \boldsymbol{\sigma}, \quad (5)$$

where m^* is the effective mass of electron, \hbar Planck's constant over 2π , k_x (k_y) the wave vector along x (y) axis, α the Rashba coefficient, $\sigma = (\sigma_x, \sigma_y)$ the vector of the Pauli matrices, $\mathbf{h} = (h_x, h_y) = \frac{1}{2}g_e\mu_B(B_x, B_y)$ is the Zeeman energies induced by the in-plane magnetic fields (B_x, B_y), with g_e the Landé g-factor, μ_B the Bohr magneton. The eigen energies and states of H_C are given by

$$\epsilon_{\pm}(\mathbf{k}) = \frac{\hbar^2}{2m^*}k^2 \pm \Lambda, \quad (6)$$

$$|+, \mathbf{k}\rangle = \begin{bmatrix} 1/\sqrt{2} \\ U \end{bmatrix}, \quad |-, \mathbf{k}\rangle = \begin{bmatrix} -U^* \\ 1/\sqrt{2} \end{bmatrix}, \quad (7)$$

where

$$U = [\alpha k_y + h_x - i(\alpha k_x - h_y)]/\sqrt{2}\Lambda, \\ \Lambda = \sqrt{(\alpha k_y + h_x)^2 + (\alpha k_x - h_y)^2}. \quad (8)$$

The valence bands in Eq. (4) are described by the isotropic (by approximating the model parameters $\gamma_2 = \gamma_3$) Kohn-Luttinger model,²⁶

$$H_V = -\frac{\hbar^2}{2m_e}[(\gamma_1 + \frac{5}{2}\gamma_2)k^2 - 2\gamma_2(\mathbf{k} \cdot \mathbf{S})^2], \quad (9)$$

where m_e is the electron mass, \mathbf{S} represents the 3/2 spin operator matrices, γ_1 and γ_2 the two model parameters, $\mathbf{k} = (k_x, k_y, k_z)$ the wave vector. For simplicity, we approximate $\langle k_z \rangle = 0$ and $\langle k_z^2 \rangle \simeq (\frac{\pi}{d})^2$ in H_V when considering the quantization along z direction of the quantum well, where d is the thickness of the quantum well. The eigen energies and states of the valence bands are given by

$$\epsilon_{1/2}(\mathbf{k}) = \epsilon_{4/3}(\mathbf{k}) = -\Delta - \frac{\hbar^2\gamma_1}{2m}(k^2 + \langle k_z^2 \rangle) \pm \frac{\hbar^2\gamma_2}{2m}\Omega, \quad (10)$$

$$|1, \mathbf{k}\rangle = \begin{pmatrix} Q \\ 0 \\ K \\ 0 \end{pmatrix}, \quad |2, \mathbf{k}\rangle = \begin{pmatrix} 0 \\ Q \\ 0 \\ -K \end{pmatrix}, \\ |3, \mathbf{k}\rangle = \begin{pmatrix} -K^* \\ 0 \\ Q \\ 0 \end{pmatrix}, \quad |4, \mathbf{k}\rangle = \begin{pmatrix} 0 \\ K^* \\ 0 \\ Q \end{pmatrix}, \quad (11)$$

where Δ is the energy gap, and

$$Q = C_v(-k^2 + 2\langle k_z^2 \rangle + \Omega), \\ K = \sqrt{3}C_v k_x^2, \\ \Omega = 2\sqrt{k^4 + \langle k_z^2 \rangle^2 - k^2\langle k_z^2 \rangle}, \\ C_v = \left[3k^4 + (k^2 - 2\langle k_z^2 \rangle - \Omega)^2\right]^{-1/2}. \quad (12)$$

We neglect the Zeeman effect in the valence bands, because the contribution to currents from holes is expected to be much

smaller than electrons considering the short charge and spin lifetimes of holes in n -type quantum wells. For simplicity, we also neglect the diamagnetic contribution,²⁷⁻²⁹ which should give qualitatively similar results as the Zeeman effect.

The interaction between the light and an electron is described by the electric-radiation interaction,²⁶

$$\hat{V}(t) = \frac{e}{m_e}\tilde{\mathbf{A}} \cdot \hat{\mathbf{p}}, \quad (13)$$

where $-e$ is the electron charge, $\hat{\mathbf{p}}$ the electron momentum operator. Under the electric dipole approximation, the vector potential $\tilde{\mathbf{A}}$ is related to the electric field of the single-frequency light by

$$\tilde{\mathbf{A}}(t) = \frac{1}{i\omega}[\mathbf{E}(\omega)e^{-i\omega t} - \mathbf{E}^*(\omega)e^{i\omega t}] \quad (14)$$

where we consider a linearly polarized single-color light incident normally to the $x-y$ plane, with the frequency ω and the polarization electric vector

$$\mathbf{E} = E_0(\cos\theta, \sin\theta, 0), \quad (15)$$

where E_0 is the amplitude and θ is the polarization angle with respect to the x axis. The electron-radiation interaction can also be expressed as

$$\hat{V}(t) = e\hat{\mathbf{r}} \cdot [\mathbf{E}(\omega)e^{-i\omega t} + \mathbf{E}^*(\omega)e^{i\omega t}], \quad (16)$$

where $\hat{\mathbf{r}}$ is the electron position operator.

In this work, we intend to focus on the microscopic physical picture. We expect that more sophisticated calculations, e.g. by using the 14-band $\mathbf{k} \cdot \mathbf{p}$ model¹⁴ or the full band structure local density approximation,³⁰ can provide a more qualitatively precise description, but will not deviate from the qualitative results obtained by using the Rashba and Kohn-Luttinger models.

B. Photoexcited carrier density

The photoexcited carrier density and all the physical quantities can be found within the density matrix formalism. In this work, we will only consider the photoexcited steady-state nonequilibrium density matrix, which can be found by the approach similar to that to the second order nonlinear optical susceptibilities.³¹ We start with the Liouville equation of the density matrix,

$$\partial_t \rho_{nm} = -\frac{i}{\hbar}[H, \hat{\rho}]_{nm} - \gamma_{nm}(\rho_{nm} - \rho_{nm}^{(0)}), \quad (17)$$

where n and m belong to the states in Eqs. (7) and (11), and γ is a phenomenological damping parameter. $\rho_{nm}^{(0)}$ is the equilibrium density matrix before the light excitation. Because we assume a n -type quantum well, the valence bands are fully occupied $\rho_{v,v'}^{(0)} = \delta_{v,v'}$, where $v, v' \in \{1, 2, 3, 4\}$. While the initial equilibrium density matrix of the conduction bands are described by the Fermi function,

$$\rho_{c,c'}^{(0)} = f_c \delta_{c,c'} \equiv \frac{1}{e^{[\epsilon_c(k) - E_F]/k_B T} + 1} \delta_{c,c'}, \quad (18)$$

where $c, c' \in \{+, -\}$, E_F the Fermi energy, k_B the Boltzmann constant, T the temperature. By treating $H_0 = H_C + H_V$ as unperturbed part and $\hat{V}(t)$ as perturbation, the perturbation equations up to the second order are given by

$$\begin{aligned}\partial_t \rho_{nm}^{(0)} &= -i\omega_{nm}\rho_{nm}^{(0)}, \\ \partial_t \rho_{nm}^{(1)} &= -i\omega_{nm}\rho_{nm}^{(1)} - \frac{i}{\hbar} [\hat{V}, \hat{\rho}^{(0)}]_{nm} - \gamma_{nm}\rho_{nm}^{(1)}, \\ \partial_t \rho_{nm}^{(2)} &= -i\omega_{nm}\rho_{nm}^{(2)} - \frac{i}{\hbar} [\hat{V}, \hat{\rho}^{(1)}]_{nm} - \gamma_{nm}\rho_{nm}^{(2)},\end{aligned}\quad (19)$$

where $\omega_{nm}(\mathbf{k}) = [\epsilon_n(\mathbf{k}) - \epsilon_m(\mathbf{k})]/\hbar$, and ρ_{nm} are functions of \mathbf{k} because the light is momentum-free under the electric dipole approximation. After a straightforward deduction, the leading order of the light induced steady-state density matrix for the conduction bands is found to be of the second order

$$\begin{aligned}\rho_{cc',\mathbf{k}}^{(2)} &= \frac{\tau_e \pi e^2}{\hbar^2 \omega^2} \sum_{\mathbf{v}} [\mathbf{v}_{c\mathbf{v}}(\mathbf{k}) \cdot \mathbf{E}(\omega)] [\mathbf{v}_{\mathbf{v}c'}(\mathbf{k}) \cdot \mathbf{E}^*(\omega)] \\ &\times [(1 - f_c)\delta(\omega - \omega_{c\mathbf{v}}) + (1 - f_{c'})\delta(\omega - \omega_{\mathbf{v}c'})],\end{aligned}\quad (20)$$

where the steady state is approximated by introducing the momentum relaxation time τ_e ,

$$\rho_{cc',\mathbf{k}}^{(2)} = \tau_e \partial_t \rho_{cc',\mathbf{k}}^{(2)}(t).\quad (21)$$

Note that Eq. (20) recovers the result by employing the semiconductor optical Bloch equations¹⁴ and Fermi's Golden rules.¹⁸ In the following, we will suppress the superscript of $\rho^{(2)}$ for simplicity.

By substituting the velocity $\mathbf{v}_{c\mathbf{v}}$ in Eq. (20) by the position $\mathbf{r}_{c\mathbf{v}}$ according to

$$\langle c, \mathbf{k} | \hat{v}_i | v, \mathbf{k} \rangle = \langle c, \mathbf{k} | \frac{1}{i\hbar} [\hat{r}_i, H_0] | v, \mathbf{k} \rangle = i\omega_{c\mathbf{v}} \langle c, \mathbf{k} | \hat{r}_i | v, \mathbf{k} \rangle, \quad (22)$$

Eq. (20) can also be expressed as

$$\begin{aligned}\rho_{cc',\mathbf{k}} &= \frac{\tau_e \pi e^2}{\hbar^2 \omega} \sum_{\mathbf{v}} [\omega_{c\mathbf{v}}(1 - f_c)\delta(\omega - \omega_{c\mathbf{v}}) \\ &+ \omega_{\mathbf{v}c'}(1 - f_{c'})\delta(\omega - \omega_{\mathbf{v}c'})] [\mathbf{r}_{c\mathbf{v}}(\mathbf{k}) \cdot \mathbf{E}(\omega)] [\mathbf{r}_{\mathbf{v}c'}(\mathbf{k}) \cdot \mathbf{E}^*(\omega)].\end{aligned}\quad (23)$$

By using the eigen states in Eqs. (7) and (11) and considering the spatial wavefunctions of the eigen states, the elements of the transition matrix $\mathbf{r}_{c\mathbf{v}} \equiv (x_{c\mathbf{v}}, y_{c\mathbf{v}}) = (x_{\mathbf{v}c}^\dagger, y_{\mathbf{v}c}^\dagger)$ are found as

$$\begin{aligned}x_{\mathbf{v}c} &\equiv \langle v, \mathbf{k} | \hat{x} | c, \mathbf{k} \rangle \\ &= a_{c\mathbf{v}} \begin{bmatrix} \frac{1}{\sqrt{2}}(\frac{K^*}{\sqrt{3}} - Q) & (Q - \frac{K^*}{\sqrt{3}})U^* \\ -(\frac{Q}{\sqrt{3}} + K^*)U & -\frac{1}{\sqrt{2}}(\frac{Q}{\sqrt{3}} + K^*) \\ \frac{1}{\sqrt{2}}(K + \frac{Q}{\sqrt{3}}) & -(K + \frac{Q}{\sqrt{3}})U^* \\ (Q - \frac{K}{\sqrt{3}})U & \frac{1}{\sqrt{2}}(Q - \frac{K}{\sqrt{3}}) \end{bmatrix}\end{aligned}\quad (24)$$

and

$$\begin{aligned}y_{\mathbf{v}c} &\equiv \langle v, \mathbf{k} | \hat{y} | c, \mathbf{k} \rangle \\ &= ia_{c\mathbf{v}} \begin{bmatrix} \frac{1}{\sqrt{2}}(Q + \frac{K^*}{\sqrt{3}}) & -(Q + \frac{K^*}{\sqrt{3}})U^* \\ (\frac{Q}{\sqrt{3}} - K^*)U & \frac{1}{\sqrt{2}}(\frac{Q}{\sqrt{3}} - K^*) \\ \frac{1}{\sqrt{2}}(\frac{Q}{\sqrt{3}} - K) & (K - \frac{Q}{\sqrt{3}})U^* \\ (\frac{K}{\sqrt{3}} + Q)U & \frac{1}{\sqrt{2}}(\frac{K}{\sqrt{3}} + Q) \end{bmatrix},\end{aligned}\quad (25)$$

where we have defined

$$a_{c\mathbf{v}} \equiv \langle 0, 0 | x | 1, -1 \rangle \quad (26)$$

with $|0, 0\rangle$ and $|1, -1\rangle$ the spherical harmonic functions $Y_{0,0}$ and $Y_{1,-1}$, respectively. U , K , and Q in Eqs. (24) and (25) have been defined in Eqs. (8) and (12). Note that the optical selection rules owing to the s and p -wave natures of the conduction and valence bands have been incorporated in Eqs. (24) and (25).

In this work, we neglect the hole contribution from the valence bands because the charge and spin lifetimes of holes are much shorter than those of electrons for n -type quantum wells.

C. Constant energy contours

In the following sections, we will use the notion of constant energy contour from time to time. It can be illustrated with the help of two spin-split conduction bands $|c = \pm, \mathbf{k}\rangle$ and a valence band $|v, \mathbf{k}\rangle$ as depicted in Fig. 2. In this work, we consider that the dominant optical excitation is the direct interband optical transition, i.e., electrons are excited from the valence bands to the conduction bands. ‘‘Direct’’ means that the wave vector \mathbf{k} of an electron does not change in the transition, while the energy of the electron is increased by a photon energy ω , as required by the momentum-energy conservation $\delta[\omega - \omega_{c\mathbf{v}}(\mathbf{k})]$ in Eq. (23). In k_x - k_y space, all the states satisfying the momentum-energy conservation form a set of constant energy contours, which are symmetric at zero magnetic field [dashed rings in Fig. 2(a)] and distorted in the presence of an in-plane magnetic field [dashed rings in Fig. 2(b)]. There is a constant energy contour for each permitted pair of a conduction band and a valence band.

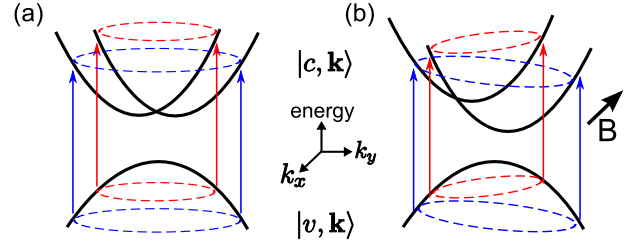


FIG. 2: (Color online) Schematic description of direct interband optical transitions from a valence band $|v, \mathbf{k}\rangle$ to the spin-split conduction bands $|c = \pm, \mathbf{k}\rangle$ at zero magnetic field (a) and in the presence of a magnetic field B (b). The states involved in the transitions form a set of constant energy contours (denoted by dashed rings), which are symmetric at zero magnetic field, and shifted along k_y (k_x) in the presence of a magnetic field along x (y) direction, where the Rashba spin-orbit coupling is assumed.

In polar coordinates [$k^2 \equiv k_x^2 + k_y^2$, $\varphi \equiv \arctan(k_y/k_x)$], the constant energy contours satisfy the equations $k = k_{c\mathbf{v}}(\varphi)$, where $k_{c\mathbf{v}}$ are the roots of $\omega = \omega_{c\mathbf{v}}(k, \varphi)$ as functions of φ . At zero magnetic field and by assuming the isotropic Rashba and Kohn-Luttinger models, $k_{c\mathbf{v}}$ are constants irrelevant to φ for each pair of conduction band $|c, \mathbf{k}\rangle$ and valence band $|v, \mathbf{k}\rangle$.

IV. ANISOTROPY OF PHOTOEXCITED CARRIER DENSITY IN \mathbf{k} SPACE

In this work, we will retain only the diagonal part of the density matrix because when ignoring the broadening of the light frequency ω , the coherent contribution from the off-diagonal part of the density matrix can be neglected.¹⁴ The diagonal terms of the density matrix have clear physical meaning as the photoexcited carrier density. By substituting the polarization electric field vector $\mathbf{E} = E_0(\cos \theta, \sin \theta)$ into Eq. (23), the carrier density excited by the linear light from valence band $|v, \mathbf{k}\rangle$ to conduction band $|c, \mathbf{k}\rangle$ as a function of the wave vector \mathbf{k} can be divided into three terms according to their dependence on the polarization angle θ ,

$$\rho_{cv, \mathbf{k}} = \rho_{cv, \mathbf{k}}^0 + \rho_{cv, \mathbf{k}}^{\cos} \cos 2\theta + \rho_{cv, \mathbf{k}}^{\sin} \sin 2\theta, \quad (27)$$

where

$$\begin{aligned} \rho_{cv, \mathbf{k}}^0 &= \frac{\tau_e \pi e^2 E_0^2}{\hbar^2} (1 - f_c) \delta(\omega - \omega_{cv}) (|x_{cv}|^2 + |y_{cv}|^2), \\ \rho_{cv, \mathbf{k}}^{\cos} &= \frac{\tau_e \pi e^2 E_0^2}{\hbar^2} (1 - f_c) \delta(\omega - \omega_{cv}) (|x_{cv}|^2 - |y_{cv}|^2), \\ \rho_{cv, \mathbf{k}}^{\sin} &= \frac{\tau_e \pi e^2 E_0^2}{\hbar^2} (1 - f_c) \delta(\omega - \omega_{cv}) \text{Re}(2x_{cv}y_{vc}). \end{aligned} \quad (28)$$

In Fig. 3, we show the numerical results for the zero-field carrier density $\rho_{cv, \mathbf{k}}$ excited by the linear light from valence band $|1, \mathbf{k}\rangle$ to conduction bands $|\pm, \mathbf{k}\rangle$ as functions of the wave vector angle φ , with φ defined as $\tan \varphi \equiv k_y/k_x$. For clarity, three terms in Eq. (27) are demonstrated separately. The first term $\rho_{cv, \mathbf{k}}^0$ is an isotropic function of φ , while $\rho_{cv, \mathbf{k}}^{\cos}$ and $\rho_{cv, \mathbf{k}}^{\sin}$ depend on $\cos 2\varphi$ and $\sin 2\varphi$, respectively, indicating the total carrier density excited by the linear light is anisotropic in \mathbf{k} space. Note that $\rho_{cv, \mathbf{k}}^0$ are always positive and overwhelm $\rho_{cv, \mathbf{k}}^{\cos, \sin}$ in magnitude, so the total photoexcited carrier density is physically positive. In addition, note that the carriers excited from the same valence band have different carrier density on conduction bands $|+, \mathbf{k}\rangle$ and $|-, \mathbf{k}\rangle$, e.g., as indicated by the ‘‘max’’ and ‘‘min’’ values of $\rho_{+, \mathbf{k}}^{0, \cos, \sin}(0)$ [Figs. 3(a1)-(c1)] and $\rho_{-, \mathbf{k}}^{0, \cos, \sin}(0)$ [Figs. 3(a2)-(c2)]. This difference is due to the splitting of the constant energy contours for $|+, \mathbf{k}\rangle$ and $|-, \mathbf{k}\rangle$ by the spin-orbit coupling, as shown in Fig. 2(a). We only show the numerical results for the carriers excited from valence bands $|1, \mathbf{k}\rangle$ to $\pm, \mathbf{k}\rangle$. Other pairs of conduction and valence bands also show similar anisotropic photoexcited carrier density in \mathbf{k} space.

Summarizing the above, the carrier density excited via direct interband transitions from valence band $|v, \mathbf{k}\rangle$ to conduction band $|c, \mathbf{k}\rangle$ by the normal incidence of a linearly polarized light can be expressed as (please refer to Appendix B for details)

$$\rho_{cv, \mathbf{k}} = \rho_{cv}^0 + \rho_{cv}^{\cos} \cos 2\varphi \cos 2\theta + \rho_{cv}^{\sin} \sin 2\varphi \sin 2\theta, \quad (29)$$

where $\rho_{cv}^{0, \cos, \sin}$ are coefficients irrelevant of φ in absence of the magnetic field for isotropic conduction and valence bands. Under a weak in-plane magnetic field (say, less than 1 Tesla),

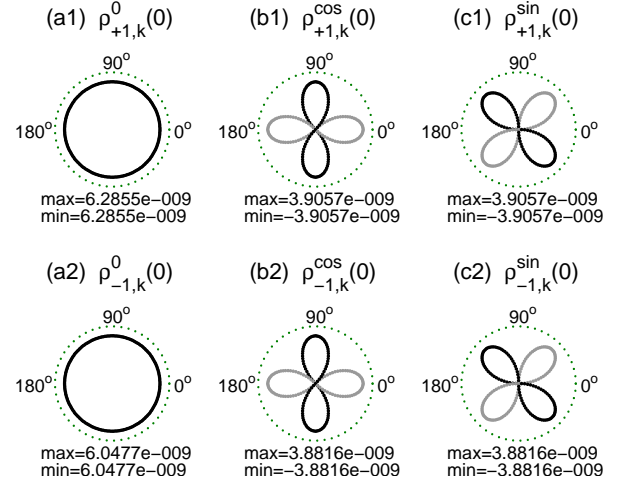


FIG. 3: (Color online) At zero magnetic field ($B_x = 0, B_y = 0$), the calculated photoexcited carrier density $\rho_{cv, \mathbf{k}}$ in Eq. (27) as functions of the wave vector angle φ in polar coordinates. Dark (light) represents positive (negative) values. ‘‘max’’ (‘‘min’’) indicates the maximum (minimum) values. $\rho_{cv, \mathbf{k}}^0$ term is always positive and overwhelms $\rho_{cv, \mathbf{k}}^{\cos/\sin}$. $\rho_{+, \mathbf{k}}^{0, \cos, \sin}$ are in units of $(2\tau_e \pi e^2 E_0^2 a_{cv}^2 / \hbar^2) \times$ (second/meter), and have a dimension of meter^{-1} . Parameters: $T = 77$ K, $E_F = 0.01$ eV, $\omega = 0.8$ eV, $m^* = 0.04m_e$, $\gamma_1 = 11.97$, $\gamma_2 = 4.36$, $\Delta = 0.76$ eV, $d = 20$ nm, $\alpha = 0.00431$ eV·nm.

$\rho_{cv}^{0, \cos, \sin}$ will also depend on φ , but with very slight changes in value.

The anisotropy of the photoexcited carrier density is the core of this paper. We will see that it naturally accounts for the behaviors of the magnetic field induced electric photocurrent²³ and the pure spin photocurrent predicted in the previous works,^{18,19} in particular the dependence on the in-plane magnetic fields and the polarization of the linearly polarized light.

V. MAGNETIC-FIELD INDUCED ELECTRIC PHOTOCURRENT

The electric photocurrent density along $\mu (\in \{x, y\})$ axis can be found by summing the velocities of the photoexcited carriers

$$j_\mu = -e \sum_{c, v, \mathbf{k}} \rho_{cv, \mathbf{k}} v_{cv, \mathbf{k}}^\mu. \quad (30)$$

From the eigen energies Eq. (6), the velocity along x and y directions for conduction bands $|\pm, \mathbf{k}\rangle$ can be found as

$$v_{\pm \mathbf{k}}^x \equiv \frac{1}{\hbar} \frac{\partial \epsilon_{\pm}}{\partial k_x} = \frac{\hbar}{m^*} k_x \pm \frac{\alpha}{\hbar} \frac{(\alpha k_x - h_y)}{\sqrt{(\alpha k_y + h_x)^2 + (\alpha k_x - h_y)^2}}. \quad (31)$$

By rewriting $k_x = k \cos \varphi$ and $k_y = k \sin \varphi$ in polar coordinates (k, φ) and expanding the velocities up to the linear order in h_x and h_y , we have

$$v_{\pm \mathbf{k}}^x \simeq \left(\frac{\hbar}{m^*} k \pm \frac{\alpha}{\hbar} \right) \cos \varphi \mp \frac{\sin 2\varphi}{2\hbar k} h_x \mp \frac{\sin^2 \varphi}{\hbar k} h_y. \quad (32)$$

$v_{cv,\mathbf{k}}^\mu$ in the current density formula (30) is related to Eq. (32) by restricting k on the constant energy contours k_{cv} .

Combining Eqs. (29) and (32), now we are ready to explain the dependence of the electric photocurrent on the polarization angle θ and magnetic fields in Eq. (1). For the current density along x direction, we rewrite the summation in Eq. (30) as an angle integral (please refer to Appendix B for details)

$$j_x = -\frac{e}{(2\pi)^2} \sum_{c,v} \int_0^{2\pi} d\varphi k_{cv} \times [\rho_{cv}^0 + \rho_{cv}^{\cos} \cos 2\varphi \cos 2\theta + \rho_{cv}^{\sin} \sin 2\varphi \sin 2\theta] \times [(\frac{\hbar}{m^*} k_{cv} + c \frac{\alpha}{\hbar}) \cos \varphi - c \frac{\sin 2\varphi}{2\hbar k_{cv}} h_x - c \frac{\sin^2 \varphi}{\hbar k_{cv}} h_y], \quad (33)$$

where $\varphi \equiv \arctan(k_y/k_x)$, $k^2 \equiv k_x^2 + k_y^2$, and $k_{cv}(\varphi)$ are the roots of $\omega = \omega_{cv}(k, \varphi)$. In general, $k_{cv}(\varphi)$ and $\rho_{cv}^{0,\cos,\sin}$ are functions of φ for finite magnetic fields, and irrelevant to φ at zero magnetic field. Note that if the full anisotropy of the conduction and valence bands is also taken into account, e.g., by employing the Kane model,³² $k_{cv}(\varphi)$ and $\rho_{cv}^{0,\cos,\sin}$ also slightly depend on φ at zero magnetic field. This slight dependence is ignored in this work, because it will not qualitatively change our microscopic physical picture.

When there is no magnetic field, the constant energy contours are perfect concentric circles in \mathbf{k} space [Fig. 2(a)], which means k_{cv} are constant for each pair of c and v . Then the integral in Eq. (33) becomes

$$j_x(0) = -\frac{e}{(2\pi)^2} \sum_{c,v} (\frac{\hbar}{m^*} k_{cv} + c \frac{\alpha}{\hbar}) k_{cv} \times \left[\rho_{cv}^0 \int_0^{2\pi} d\varphi \cos \varphi + \rho_{cv}^{\cos} \cos 2\theta \int_0^{2\pi} d\varphi \cos \varphi \cos 2\varphi + \rho_{cv}^{\sin} \sin 2\theta \int_0^{2\pi} d\varphi \cos \varphi \sin 2\varphi \right], \quad (34)$$

where all the above integrals over φ yield zero, which explains why no current can be induced in absence of a magnetic field from a mathematical viewpoint.

A. Current induced by a parallel magnetic field

As depicted by Eq. (1), when a magnetic field is applied parallel to the current measurement direction, a current proportional to $\sin 2\theta$ can be observed. According to the energy spectra of the conduction bands in Eq. (6) and Fig. 2(b), a magnetic field can only induce a shift of wave vectors along direction perpendicular to the magnetic field, so the current induced by the parallel magnetic field seems counter-intuitive at the first sight.

According to Eq. (32), the parallel magnetic field B_x varies the velocity in x direction by

$$\Delta v_{\pm\mathbf{k}}^x(B_x) \equiv v_{\pm\mathbf{k}}^x(B_x) - v_{\pm\mathbf{k}}^x(0) \simeq \mp \frac{\sin 2\varphi}{2\hbar k} h_x, \quad (35)$$

which leads to the following three integrals in Eq. (33),

$$j_x(B_x) \simeq 2\eta h_x \frac{e}{(2\pi)^2} \sum_{c,v} \frac{c}{2\hbar}$$

$$\times \left[\rho_{cv}^0 \int_0^{2\pi} d\varphi \sin 2\varphi + \rho_{cv}^{\cos} \cos 2\theta \int_0^{2\pi} d\varphi \cos 2\varphi \sin 2\varphi + \rho_{cv}^{\sin} \sin 2\theta \int_0^{2\pi} d\varphi \sin 2\varphi \sin 2\varphi \right], \quad (36)$$

where the extra “ 2η ” account for the dependence of $\rho_{cv}^{0,\cos,\sin}$ and k_{cv} on φ , and will be explained in Sec. VD. The only nonzero integral in Eq. (36) is the last term, which gives

$$j_x(B_x) \simeq \eta h_x \frac{e}{4\pi\hbar} \sum_{c,v} c \rho_{cv}^{\sin} \sin 2\theta. \quad (37)$$

This contributes to the $c_x B_x \sin 2\theta$ term in Eq. (1), and means that in the presence of the $\sin 2\varphi$ -dependent anisotropic photoexcited carrier density, a parallel magnetic field B_x do induce a current proportional to $\sin 2\theta$.

B. Current induced by a perpendicular magnetic field

According to Eq. (1), a perpendicular magnetic field B_y can induce two terms of the electric photocurrent, one is irrelevant to θ , and the other is proportional to $\cos 2\theta$.

As given in Eq. (32), the perpendicular magnetic field B_y varies the velocity along x axis by

$$\Delta v_{\pm\mathbf{k}}^x(B_y) \equiv v_{\pm\mathbf{k}}^x(B_y) - v_{\pm\mathbf{k}}^x(0) \simeq \mp \frac{\sin^2 \varphi}{\hbar k} h_y, \quad (38)$$

which gives rise to the following three integrals in Eq. (33),

$$j_x(B_y) \simeq 2\eta h_y \frac{e}{(2\pi)^2} \sum_{c,v} \frac{c}{\hbar} \times \left[\rho_{cv}^0 \int_0^{2\pi} d\varphi \sin^2 \varphi + \rho_{cv}^{\cos} \cos 2\theta \int_0^{2\pi} d\varphi \cos 2\varphi \sin^2 \varphi + \rho_{cv}^{\sin} \sin 2\theta \int_0^{2\pi} d\varphi \sin 2\varphi \sin^2 \varphi \right], \quad (39)$$

where the extra “ 2η ” account for the dependence of $\rho_{cv}^{0,\cos,\sin}$ and k_{cv} on φ , and will be explained in Sec. VD. The first two integrals in Eq. (39) are nonzero. They gives

$$j_x(B_y) \simeq \eta h_y \frac{e}{2\pi\hbar} \sum_{c,v} c \rho_{cv}^0 - \eta h_y \frac{e}{4\pi\hbar} \sum_{c,v} c \rho_{cv}^{\cos} \cos 2\theta, \quad (40)$$

which contribute to the $c_0 B_y$ and $c_y B_y \cos 2\theta$ terms in Eq. (1).

C. Microscopic physical picture in \mathbf{k} space

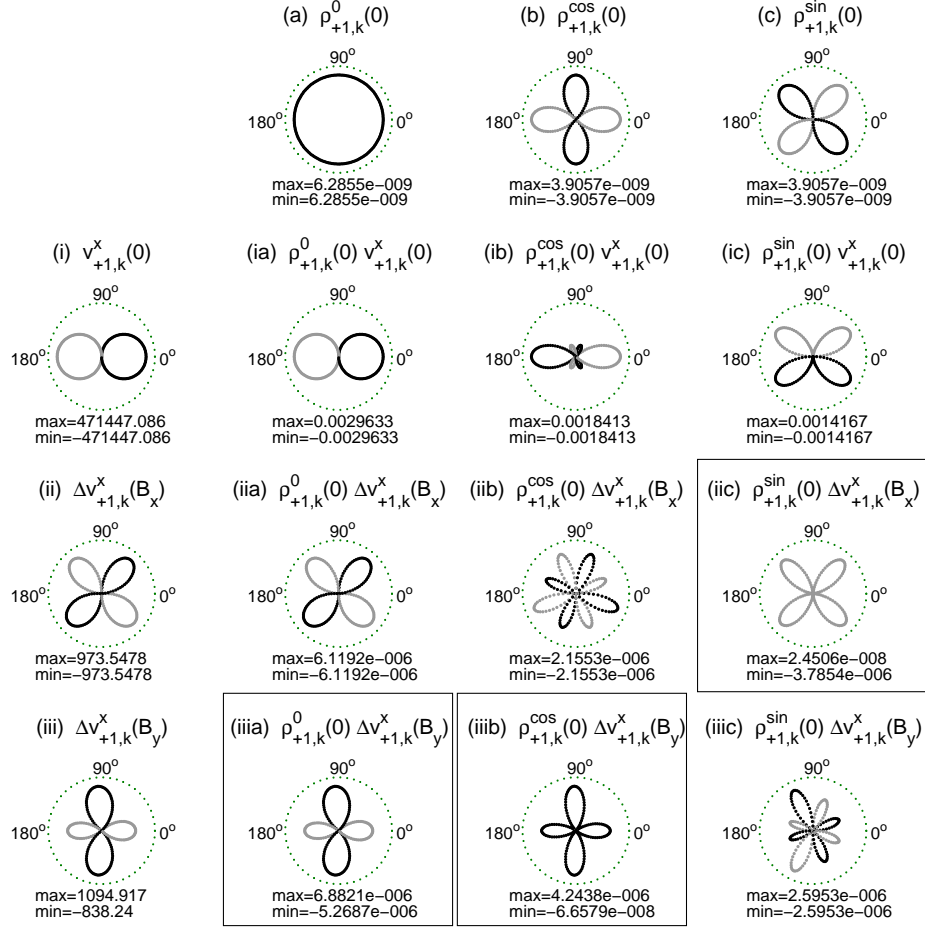


FIG. 4: (Color online) The product table of the density and velocity of the photoexcited carriers excited from valence band $|1, \mathbf{k}\rangle$ to conduction band $|+, \mathbf{k}\rangle$ as functions of wave vector angle φ in polar coordinates. [(a)-(c)] The photoexcited carrier density $\rho_{+1,\mathbf{k}}^{0,\text{cos},\text{sin}}$ at zero magnetic field. [(i)-(iii)] The velocity of the photoexcited carriers at zero magnetic field (i), and the variation of the velocity in the presence of a magnetic field along x (ii) and y (iii) directions, respectively. “(0)” stands for the values in absence of the magnetic field, and “ $\Delta\dots(B_\nu)$ ” for the variation upon applying the magnetic field B_ν along ν direction. Dark (light) represents positive (negative) values. “max” (“min”) indicates the maximum (minimum) values along radial direction. $\rho_{+1,\mathbf{k}}^{0,\text{cos},\text{sin}}$ shown here are in units of $(2\tau_e\pi e^2 E_0^2 a_{cv}^2 / \hbar^2) \times (\text{second}/\text{meter})$, and have a dimension of meter^{-1} . The velocities are related to Eq. (32) by letting $k = k_{+1}$ on the constant energy contour between $|1, \mathbf{k}\rangle$ and $|+, \mathbf{k}\rangle$, and are in units of $\text{meter}/\text{second}$. The boxes mark the origins of the three terms in Eq. (1). $g_e = -4$, other parameters are the same as those in Fig. 3.

The microscopic physical picture of above integrals can be found in Fig. 4, where we give a product table of the velocity along x axis and the photoexcited carrier density for the carriers excited from $|1, \mathbf{k}\rangle$ to $|+, \mathbf{k}\rangle$ as functions of wave vector angle φ in polar coordinates. The three nonzero contributions in Eqs. (37) and (40) are marked by the boxes in sub-figures (iic), (iiia), and (iiib). Besides the three nonzero terms, note that all the other sub-figures in Fig. 4 have the similar feature, i.e., they always have equal weight of positive and negative lobes. Thus, their summations over φ give no contribution to the electric current. Note that in Fig. 4 only the results for the carriers excited from $|1, \mathbf{k}\rangle$ to $|+, \mathbf{k}\rangle$ are demonstrated. The rest seven pairs of conduction and valence bands yield similar result, and all of them add up to the total net electric current. Note that the numerical result of $v_{cv,\mathbf{k}}^x(B_y)$ [Fig. 4(iii)]

is actually not consistent with the form of $\sin^2 \varphi$. The extra lobes along 0° and 180° are due to the shift of constant energy contours along k_x direction induced by B_y , which can be incorporated in Eq. (39) by considering k_{cv} as a function of φ .

D. Contribution from magnetic field induced variation in photoexcited carrier density

In the above discussions we have neglected the dependence of k_{cv} and $\rho_{cv}^{0,\text{cos},\text{sin}}$ on φ at finite magnetic fields, i.e., the variation of the photoexcited carrier density upon applying the magnetic field. Under the magnetic fields, we can write the photoexcited carrier density and velocity along μ direction as

$$\rho_{cv,\mathbf{k}}(B_\nu) = \rho_{cv,\mathbf{k}}(0) + \Delta\rho_{cv,\mathbf{k}}(B_\nu),$$

$$v_{\mathbf{c}\mathbf{k}}^{\mu}(B_{\nu}) = v_{\mathbf{c}\mathbf{k}}^{\mu}(0) + \Delta v_{\mathbf{c}\mathbf{k}}^{\mu}(B_{\nu}), \quad (41)$$

where “(0)” stands for the values in absence of the magnetic field, and “ $\Delta \dots(B_{\nu})$ ” for the variation upon applying the magnetic field B_{ν} along ν direction. The charge current j_{μ} induced by B_{ν} can be expanded as

$$j_{\mu}(B_{\nu}) \simeq -e \sum_{c,v,\mathbf{k}} [\rho_{c\nu,\mathbf{k}}(0)v_{\mathbf{c}\mathbf{k}}^{\mu}(0) + \rho_{c\nu,\mathbf{k}}(0)\Delta v_{\mathbf{c}\mathbf{k}}^{\mu}(B_{\nu}) + \Delta \rho_{c\nu,\mathbf{k}}(B_{\nu})v_{\mathbf{c}\mathbf{k}}^{\mu}(0) + \Delta \rho_{c\nu,\mathbf{k}}(B_{\nu})\Delta v_{\mathbf{c}\mathbf{k}}^{\mu}(B_{\nu})] + O(B_{\nu}^2), \quad (42)$$

where we already illustrated that the first term on the right gives nothing, while the second term is found to be consistent with experimentally observed the magnetic field induced photocurrent (Secs. V A and V B). Besides, one can expect that the third term, i.e., the magnetic field induced variation of the photoexcited carrier density, gives a contribution of the same

order as the second term, and the last term is ignorably small. Therefore, we roughly approximate the photocurrent density induced by the magnetic field by

$$j^{\mu}(B_{\nu}) \simeq -2\eta e \sum_{c,v,\mathbf{k}} \rho_{c\nu,\mathbf{k}}(0)\Delta v_{\mathbf{c}\mathbf{k}}^{\mu}(B_{\nu}), \quad (43)$$

which gives the extra “ 2η ” in front of Eqs. (36) and (39). We numerically check that η depends on parameters sensitively, but is basically of order of 1.

VI. SPIN PHOTOCURRENT AT ZERO MAGNETIC FIELD

A. Pure spin photocurrent at zero magnetic field

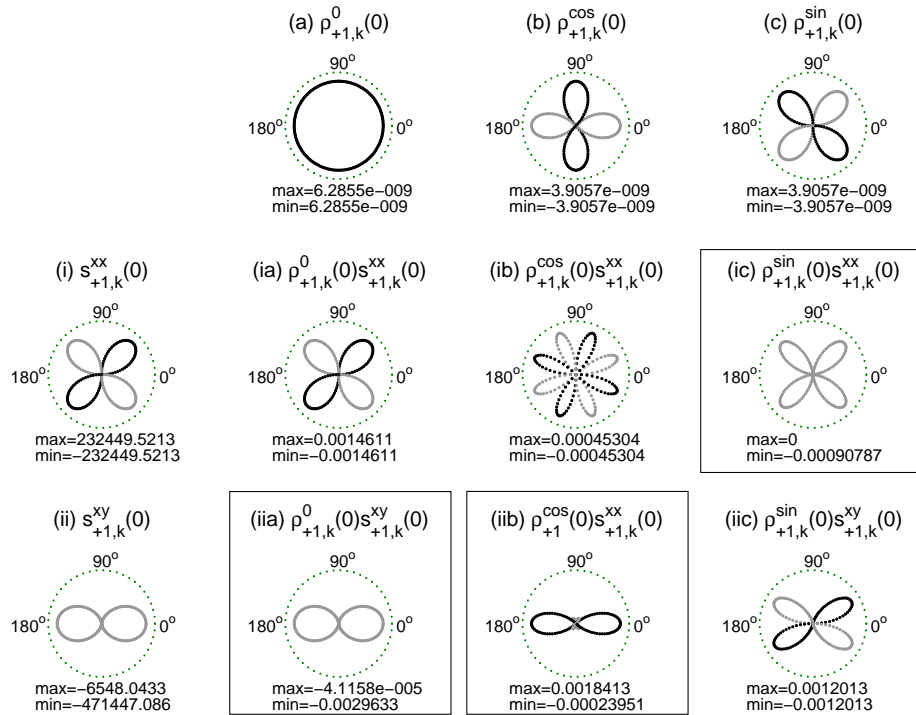


FIG. 5: (Color online) The product table of the density and spin velocities of the carriers excited from valence band $|1, \mathbf{k}\rangle$ to conduction band $|+1, \mathbf{k}\rangle$ as functions of wave vector angle φ in polar coordinates at zero magnetic field. [(a)-(c)] The photoexcited carrier density $\rho_{+1,\mathbf{k}}$. [(i)-(ii)] The spin velocity of the photoexcited carriers flowing along x axis with spin pointing along x [(i)] and y [(ii)] directions, respectively. Dark (light) represents positive (negative) values. “max” (“min”) indicates the maximum (minimum) values. $\rho_{+1,\mathbf{k}}^{0,\cos,\sin}$ shown here are in units of $(2\tau_e\pi e^2 E_0^2 a_{cv}^2 / \hbar^2) \times (\text{second}/\text{meter})$, and have a dimension of meter^{-1} . The spin velocities are related to Eq. (47) by letting $k = k_{+1}$ on the constant energy contour between $|1, \mathbf{k}\rangle$ and $|+1, \mathbf{k}\rangle$, and are in units of $\text{meter}/\text{second}$. The boxes mark the origins of the three terms in Eq. (44). The parameters are the same as those in Fig. 3.

As discussed in Sec. V, no electric photocurrent can be generated at zero magnetic field. However, both the symmetry argument of the $C_{2\nu}$ group¹⁵ and theoretical calculations^{14,18,19} have pointed out that pure spin currents can be induced by the

linearly polarized or unpolarized lights, and can be expressed as functions of the polarization angle θ ,

$$\vec{j}^{\mu} = I_0^{\mu} + I_1^{\mu} \cos 2\theta, \quad j^{\mu} = I_2^{\mu} \sin 2\theta, \quad (44)$$

where $I_{0,1,2}^\mu$ are constant coefficients, $\mu \in \{x, y\}$, and $\bar{\mu} = y$ if $\mu = x$, vice versa. In this section, we will show that how the anisotropy of the photoexcited carrier density is related to the θ -dependence of the pure spin current.

The spin photocurrent density flowing along $\mu \in \{x, y\}$ direction with spin polarized along $\nu \in \{x, y\}$ direction can be found by

$$J_\mu^\nu = \frac{\hbar}{2} \sum_{c,v,\mathbf{k}} \rho_{cv,\mathbf{k}} s_{cv,\mathbf{k}}^{\mu\nu}, \quad (45)$$

where we also retain only the diagonal density matrix, and $s_{cv,\mathbf{k}}^{\mu\nu}$ is the spin velocity for the carriers excited from valence band $|v, \mathbf{k}\rangle$ to conduction band $|c, \mathbf{k}\rangle$. The spin velocity operator is defined as

$$\hat{s}^{\mu\nu} = \frac{1}{2} \left\{ \sigma_\nu, \frac{1}{\hbar} \frac{\partial H_C}{\partial k_\mu} \right\}, \quad (46)$$

where σ_ν is the ν -component Pauli matrix. The zero magnetic field expectation value of the spin velocity for conduction band $|c, \mathbf{k}\rangle$, defined as $s_{\pm\mathbf{k}}^{\mu\nu} \equiv \langle \pm, \mathbf{k} | \hat{s}^{\mu\nu} | \pm, \mathbf{k} \rangle$, can be found in polar coordinates as,

$$\begin{aligned} s_{\pm\mathbf{k}}^{xx} &= \pm \frac{\hbar}{2m^*} k \sin 2\varphi, & s_{\pm\mathbf{k}}^{xy} &= \mp \frac{\hbar}{m^*} k \cos^2 \varphi - \frac{\alpha}{\hbar}, \\ s_{\pm\mathbf{k}}^{yx} &= \pm \frac{\hbar}{m^*} k \sin^2 \varphi + \frac{\alpha}{\hbar}, & s_{\pm\mathbf{k}}^{yy} &= \mp \frac{\hbar}{2m^*} k \sin 2\varphi. \end{aligned} \quad (47)$$

$s_{\pm\mathbf{k}}^{\mu\nu}$ in the spin current density formula (45) is related to Eq. (47) by restricting k on the constant energy contours between valence band $|v, \mathbf{k}\rangle$ and conduction band $|c, \mathbf{k}\rangle$.

Similar to the current density, the spin current density can also be rewritten into an angle integral,

$$\begin{aligned} j_\mu^\nu(0) &= \frac{\hbar}{2} \frac{1}{(2\pi)^2} \sum_{c,v} k_{cv} \int_0^{2\pi} d\varphi s_{cv}^{\mu\nu}(k_{cv}, \varphi) \\ &\times \left[\rho_{cv}^0 + \rho_{cv}^{\cos} \cos 2\varphi \cos 2\theta + \rho_{cv}^{\sin} \sin 2\varphi \sin 2\theta \right], \end{aligned} \quad (48)$$

where k_{cv} and $\rho_{cv}^{0,\cos,\sin}$ are irrelevant to φ at zero magnetic field, as discussed above. Similar to the angle integrals over φ in Sec. V, the polarization angle dependence of the spin currents are found as

$$j_x^x(0) = \frac{\hbar}{2} \frac{1}{4\pi} \sin 2\theta \sum_{c,v} c \frac{\hbar}{2m^*} k_{cv}^2 \rho_{cv}^{\sin}, \quad (49)$$

and

$$\begin{aligned} j_x^y(0) &= -\frac{\hbar}{2} \frac{1}{2\pi} \sum_{c,v} \left[c \frac{\hbar}{2m^*} k_{cv}^2 \rho_{cv}^0 + \frac{\alpha}{\hbar} \rho_{cv}^0 k_{cv} \right] \\ &\quad - \frac{\hbar}{2} \frac{1}{2\pi} \sum_{c,v} c \frac{1}{2} \frac{\hbar}{2m^*} k_{cv}^2 \rho_{cv}^{\cos} \cos 2\theta, \end{aligned} \quad (50)$$

which give the θ dependence in Eq. (44). The microscopic physical picture of the relation between the anisotropy of the photoexcited carrier density in \mathbf{k} space and the polarization angle θ dependence of the pure spin current is clearly shown in Fig. 5, where the nonzero contributions to Eq. (44) are marked by the boxes.

B. Quick estimate of zero-field spin photocurrent by field-induced electric photocurrent

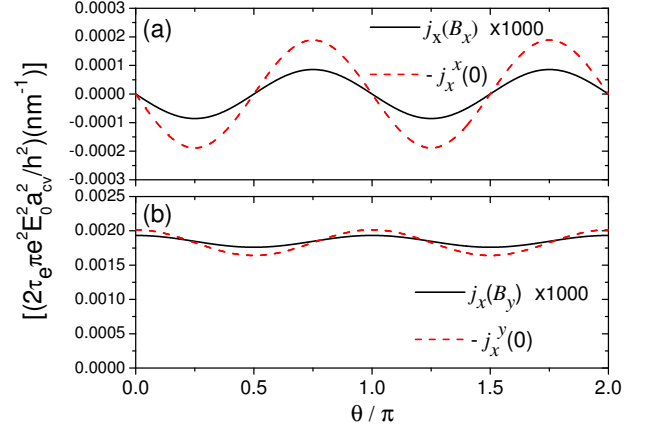


FIG. 6: (Color online) Numerical comparisons between the electric photocurrents induced by finite magnetic fields and pure spin photocurrents at zero magnetic field. (a) $j_x(B_x) \times 1000$ at $B_x = 1$ T and $-j_x^x(0)$. (b) $j_x(B_y) \times 1000$ at $B_y = 1$ T and $-j_x^y(0)$. $g_e = -4$. Other parameters are the same as those in Fig. 3. For a direct comparison, we neglect the $-e$ and $\hbar/2$ in front of the current density and spin current density formulas. The above values of currents are in units of $(2\tau_e \pi e^2 E_0^2 a_{cv}^2 / \hbar^2) \times (\text{nm}^{-1})$, and have a dimension of $\text{second}^{-1} \text{meter}^{-1}$.

Because both the magnetic field induced electric photocurrents and the zero-field pure spin photocurrents originate from the same photoexcited carrier density, this allows us to find a relation between them. With the help of Eqs. (37) and (49), the ratio between the zero-field longitudinal pure spin photocurrent and the electric photocurrent induced by the parallel magnetic field turns out to be

$$\frac{j_x^x(0)}{j_x(B_x)} \simeq -\frac{\sum_{c,v} c \rho_{cv}^{\sin} \frac{\hbar^2 k_{cv}^2}{2m^*}}{\eta \hbar_x \sum_{c,v} c \rho_{cv}^{\sin}}. \quad (51)$$

With Eqs. (40) and (50), the ratio between the transverse spin photocurrent and the perpendicular magnetic field induced electric photocurrent is given by

$$\begin{aligned} \frac{j_x^y(0)}{j_x(B_y)} &\simeq \sum_{c,v} \left[c \rho_{cv}^0 \frac{\hbar^2 k_{cv}^2}{2m^*} + \alpha \rho_{cv}^0 k_{cv} \right. \\ &\quad \left. + \frac{1}{2} \cos 2\theta c \rho_{cv}^{\cos} \frac{\hbar^2 k_{cv}^2}{2m^*} \right] \\ &\quad \left/ \eta \hbar_y \sum_{c,v} \left[c \rho_{cv}^0 - \frac{1}{2} \cos 2\theta c \rho_{cv}^{\cos} \right] \right. \end{aligned} \quad (52)$$

These relations have clear physical meaning. Note that $\sum_{c=\pm} c \rho_{cv}^{0,\cos,\sin} = \rho_{+v}^{0,\cos,\sin} - \rho_{-v}^{0,\cos,\sin}$. This difference between the photoexcited carrier density for the + and - conduction bands, as already shown in Fig. 3, is due to the spin-orbit

coupling. Therefore, the denominators in Eqs. (51) and (52) mean that both the magnetic field and the spin-orbit coupling are necessary ingredients of the field-induced electric photocurrent, while the numerators indicate that the pure spin currents are proportional to the spin-orbit coupling and the kinetic energy of the photoexcited carriers (if we can view literally $\hbar^2 k_{cv}^2/2m^*$ as kinetic energy).

At this moment, we make a bold approximation by canceling the effect of the spin-orbit coupling from both the denominators and numerators in Eqs. (51) and (52), and literally say that the ratio between the zero-field pure spin photocurrent and the field-induced electric photocurrent is about “*kinetic energy over Zeeman energy*”. This relation, though rather coarse, can help us to make a quick order-of-magnitude estimate of the undetectable pure spin photocurrent from the measured field-induced electric photocurrent.²³ The average kinetic energy of the carriers is higher than the Fermi energy measured from the bottom of the conduction bands, thus is more than $E_F = 0.01$ eV for our numerical calculations. The Zeeman energy induced by 1 tesla of magnetic field is about 10^{-4} eV for the Landé g-factor of $g_e = -4$.³²⁻³⁴ Therefore, the rough estimate implies that the spin photocurrent is more than two orders larger than the electric photocurrents induced by a magnetic field of 1 Tesla. To test the reliability of this quick estimate, we numerically compare the magnetic field induced photocurrent and pure spin photocurrent at zero magnetic field in Fig. 6. Apparently, the spin photocurrents are about three orders larger than the electric photocurrents induced by 1 Tesla of magnetic field. Despite of its roughness, this quick estimate gives reasonable result. We expect that this quick estimate may provide a reference for more sophisticated non-destructive approaches, such as the Voigt effect and the Faraday rotation³⁵ or the second-order nonlinear optical effects.³⁶

VII. CONCLUSIONS

In this work, we present a theoretical description of the recent experiment²³ on the optical injection of spin-polarized carriers via direct interband optical excitations into a semiconductor quantum well under the normal incidence of linearly polarized or unpolarized lights. In that experiment, the injection produces pure spin photocurrents accompanying no electric current at zero magnetic field due to the time-reversal symmetry. An in-plane magnetic field can break the time-reversal symmetry, and extracts a field-induced electric photocurrent. The field-induced electric photocurrent is characterized by its dependence on the magnetic fields and the polarization of the light.

With the help of the density matrix formalism, we calculate the photoexcited carrier density, current density, and spin current density. We find that the photoexcited carrier density in \mathbf{k} space shows an anisotropic dependence on both the wave vector angle φ and the polarization angle θ of the linearly polarized light as given in Eq. (29). Since the velocities of carriers can also be expressed as functions of φ [see Eq. (32)], we can show that the current density can be simplified as an

angle integral over φ of the product of the density and velocity of photoexcited carriers. The angle integral then produces all the magnetic field and polarization angle dependences of the field-induced electric current as reported in Ref. 23.

We further show that the origin of the previously predicted pure spin photocurrents^{18,19} can be well illustrated from the same photoexcited carrier density. We propose that the ratio of magnitude between the zero-field pure spin photocurrent and the field-induced electric photocurrent can be approximated as “*kinetic energy over Zeeman energy*”. With this relation, the underlying pure spin photocurrent can be quickly estimated from the observed field-induced electric photocurrent.

VIII. ACKNOWLEDGEMENTS

We thank Xiaodong Cui, Junfeng Dai, Chun-Lei Yang, Wei-Qiang Chen, Jing Wang, and Bang-fen Zhu for helpful discussions. This work was supported by the Research Grant Council of Hong Kong under Grant Nos. HKU7041/07P, and HKU 10/CRF/08. Z.B. was supported by National Natural Science Foundation of China (Grant No. 10974046) and Hubei Provincial Natural Science Foundation of China (Grant No. 2009CDB360).

Appendix A: Physical picture of C_{2v} group

It is well known that the heterostructures of inversion-asymmetric zinc blende materials grown along [001] direction have C_{2v} point group symmetry. The basic building block of these structures is shown in Fig. 7(a). It has four symmetry operations. When x and y axes are defined as $[1\bar{1}0]$ and $[110]$ crystallographic directions, respectively, the xz and yz planes coincide with the mirror reflection planes of the C_{2v} group. As the basis functions, the polar vectors (such as velocity, current, electric field) along x axis and the axial vectors (such as spin and magnetic field) along y axis transform according to the irreducible representation B_1 of the C_{2v} group, while the polar vectors along y and the axial vectors along x directions according to the irreducible representation B_2 .³⁷ The physical picture of “vectors transforming according to irreducible representations” is schematically illustrated in Fig. 7(b).

The basic observation to the experiment data indicates that the current is linearly proportional to the magnetic field, and the 2θ function dependence usually implies a second-order nonlinear optics. Phenomenologically, the current density j_α can be generally written as²¹

$$j_\alpha = \chi^{\alpha\beta\gamma\delta} B_\beta E_\gamma E_\delta, \quad (\text{A1})$$

where $\alpha, \beta, \gamma,$ and δ stand for Cartesian coordinates. B_β and E_γ are the components of the magnetic field and polarization electric field vector. The nonzero terms of Eq. (A1) require that the vectors on both sides transform in the same manner for all the symmetry operations of the C_{2v} group. Two examples are illustrated in Tab. I. In the language of the irreducible

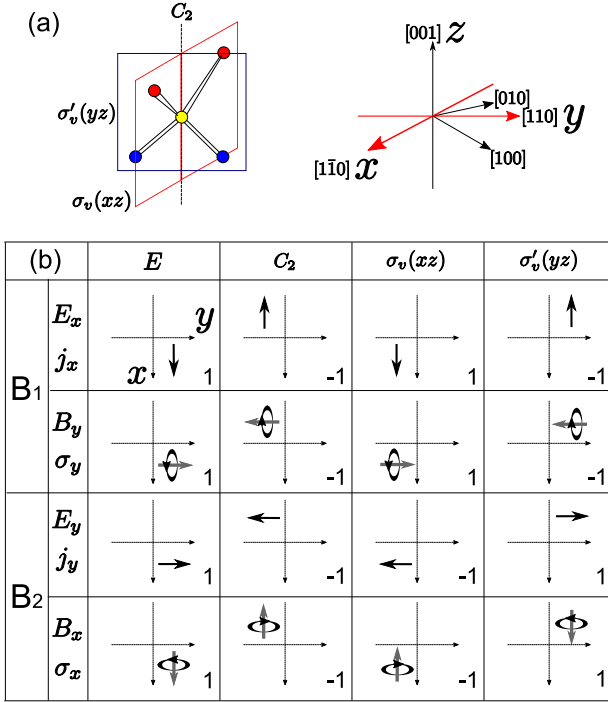


FIG. 7: (a) The building block of an inversion-asymmetric zinc blende structure grown along $[001]$ crystallographic direction. When x and y axes are defined along $[1\bar{1}0]$ and $[110]$ crystallographic directions, the xz and yz planes coincide with the mirror reflection planes of the C_{2v} point group. (b) How polar vectors j_x , j_y , E_x , E_y and axial vector B_x , B_y , σ_x , σ_y transform under the four symmetry operations of the C_{2v} point group. E : identical; C_2 : two-fold rotation about z axis; σ_v (σ'_v): mirror reflection with respect to xz (yz) plane. Whether the vector changes sign under the symmetry operator is indicated on the lower right corner of each panel by “1” or “-1”, which are actually the characters of the representations B_1 and B_2 of the C_{2v} group.³⁷

representation of group theory, the table I can be written as

$$\begin{aligned} B_1 &\neq B_2 \otimes B_1 \otimes B_1, \\ B_1 &= B_2 \otimes B_1 \otimes B_2. \end{aligned} \quad (A2)$$

Similarly, all the nonzero terms can be found and summarized as Eq. (2).

In addition, both σ_x and k_y transform according to B_1 , while $B_1 \otimes B_1$ yields the identity representation of the C_{2v} group, so $\sigma_x k_y$ is an invariant for structures with the C_{2v} symmetry. Similarly, $\sigma_y k_x$ is also an invariant. On the contrary, $\sigma_x k_x$ and $\sigma_y k_y$ are not invariants. As a result, the spin-orbit coupling up to the linear order in \mathbf{k} can be generally described by the form

$$H_{\text{SOC}} = \alpha_x \sigma_y k_x - \alpha_y \sigma_x k_y. \quad (A3)$$

Without loss of generality, we will adopt the Rashba model

$$H_{\text{R}} = \alpha(\sigma_x k_y - \sigma_y k_x). \quad (A4)$$

Note that this result only applies for when x and y directions are referred to the $[1\bar{1}0]$ and $[110]$ crystallographic directions.^{24,25} Besides, we expect that the general case that

TABLE I: Two examples of how to determine whether an element of the pseudo tensor $\chi^{\alpha\beta\gamma\delta}$ is nonzero. 1 and -1 correspond to “remaining unchanged” and “changing sign”, respectively, upon applying the symmetry operations of C_{2v} group to the vectors. (a) for χ^{xxxx} , which is zero because j_x and $B_x E_x E_x$ are different for σ_v and σ'_v . (b) for χ^{xxyy} , which is nonzero because j_x and $B_x E_x E_y$ are the same for all symmetry operations.

(a)	j_x	B_x	E_x	E_x	$B_x E_x E_x$
C_2	-1	-1	-1	-1	-1
σ_v	1	-1	1	1	-1
σ'_v	-1	1	-1	-1	1

(b)	j_x	B_x	E_x	E_y	$B_x E_x E_y$
C_2	-1	-1	-1	-1	-1
σ_v	1	-1	1	-1	1
σ'_v	-1	1	-1	1	-1

$|\alpha_x| \neq |\alpha_y|$ may account for the anisotropy of photocurrents, e.g. $J_x(B_x) \neq J_y(B_y)$, in experiments.

Appendix B: From summation over \mathbf{k} to angle integral over φ

In polar coordinates, we can write $\rho_{c\nu, \mathbf{k}}$ in Eq. (27) as

$$\rho_{c\nu, \mathbf{k}} \equiv F(k, \varphi) \delta[\omega - \omega_{c\nu}(k, \varphi)], \quad (B1)$$

where $F(k, \varphi)$ is a function of dimension of second⁻¹, and the delta function of ω can be transformed into that of k ,

$$\begin{aligned} \delta[\omega - \omega_{c\nu}(k, \varphi)] &= \frac{1}{|d\omega_{c\nu}(k, \varphi)/dk|} \Big|_{k=k_{c\nu}(\varphi)} \delta[k - k_{c\nu}(\varphi)] \\ &\equiv G[k_{c\nu}(\varphi)] \delta[k - k_{c\nu}(\varphi)], \end{aligned} \quad (B2)$$

where $k_{c\nu}(\varphi)$ are the roots of $\omega = \omega_{c\nu}(k, \varphi)$ as functions of φ . For convenience, we have defined $G[k_{c\nu}(\varphi)]$ as a function of $k_{c\nu}$. $G[k_{c\nu}(\varphi)]$ is of dimension of second meter⁻¹. At zero magnetic field, $k_{c\nu}$ is irrelevant to φ , because according to Eqs. (6) and (10) $\omega_{c\nu}$ is a function of just one variable k when $(h_x, h_y) = 0$. By performing an integral over k ,

$$\int_0^\infty k dk \rho_{c\nu, \mathbf{k}} = k_{c\nu}(\varphi) F[k_{c\nu}(\varphi), \varphi] G[k_{c\nu}(\varphi)], \quad (B3)$$

in which, considering the numerical results in Fig. 3 we can define

$$\begin{aligned} &F[k_{c\nu}(\varphi), \varphi] G[k_{c\nu}(\varphi)] \\ &\equiv \rho_{c\nu}^0(\varphi) + \rho_{c\nu}^{\cos}(\varphi) \cos 2\varphi \cos 2\theta + \rho_{c\nu}^{\sin}(\varphi) \sin 2\varphi \sin 2\theta, \end{aligned} \quad (B4)$$

where $\rho_{c\nu}^{0, \cos, \sin}$ are functions of φ at finite magnetic fields, and are irrelevant of φ at zero magnetic field. Note that $\rho_{c\nu}^{0, \cos, \sin}$ are of dimension of meter⁻¹.

Similarly, the current density formula in Eq. (30) can be written as an integral in polar coordinates,

$$\begin{aligned} j_\mu &= -e \sum_{c, \nu} \frac{1}{(2\pi)^2} \int_0^{2\pi} d\varphi \int_0^\infty k dk \\ &\quad \times F(k, \varphi) G[k_{c\nu}(\varphi)] \delta[k - k_{c\nu}(\varphi)] v_{c\nu, \mathbf{k}}^\mu \end{aligned} \quad (B5)$$

One can check that the part on the right side of the equation is of dimension of Ampere/meter. By performing the integral over k ,

$$\begin{aligned} j_\mu &= -\frac{e}{(2\pi)^2} \sum_{c,v} \int_0^{2\pi} d\varphi k_{cv} F(k_{cv}, \varphi) G[k_{cv}(\varphi)] v_{cv}^\mu(k_{cv}, \varphi) \\ &= -\frac{e}{(2\pi)^2} \sum_{c,v} \int_0^{2\pi} d\varphi k_{cv} [\rho_{cv}^0(\varphi) + \rho_{cv}^{\cos}(\varphi) \cos 2\varphi \cos 2\theta \\ &\quad + \rho_{cv}^{\sin}(\varphi) \sin 2\varphi \sin 2\theta] v_{cv}^\mu(k_{cv}, \varphi). \end{aligned} \quad (\text{B6})$$

where $v_{cv}^\mu(k_{cv}, \varphi)$ is found by letting $k = k_{cv}$ in Eq. (32). Now the summation over \mathbf{k} is converted into an angle integral over φ .

With the help of Eq. (43), the above current density can be approximately calculated from the photoexcited density at zero magnetic field by

$$\begin{aligned} j_\mu &\simeq -\frac{2\eta e}{(2\pi)^2} \sum_{c,v} \int_0^{2\pi} d\varphi k_{cv} [\rho_{cv}^0(0) + \rho_{cv}^{\cos}(0) \cos 2\varphi \cos 2\theta \\ &\quad + \rho_{cv}^{\sin}(0) \sin 2\varphi \sin 2\theta] v_{cv}^\mu(k_{cv}, \varphi). \end{aligned} \quad (\text{B7})$$

According to Secs. VA and VB, we know that the above integral has two nonzero contributions for the current density along x direction,

$$\begin{aligned} &j_x(B_x, B_y) \\ &\simeq -\frac{2\eta e}{(2\pi)^2} \sum_{c,v} \int_0^{2\pi} d\varphi k_{cv} \rho_{cv}^{\sin}(0) \sin 2\varphi \sin 2\theta \Delta v_{cv}^x(k_{cv}, \varphi, B_x) \\ &\quad -\frac{2e}{(2\pi)^2} \sum_{c,v} \int_0^{2\pi} d\varphi k_{cv} [\rho_{cv}^0(0) + \rho_{cv}^{\cos}(0) \cos 2\varphi \cos 2\theta] \\ &\quad \times \Delta v_{cv}^x(k_{cv}, \varphi, B_y). \end{aligned} \quad (\text{B8})$$

where $\Delta v_{cv}^x(k_{cv}, \varphi, B_x)$ and $\Delta v_{cv}^x(k_{cv}, \varphi, B_y)$ can be found by letting $k = k_{cv}$ in Eqs. (35) and (38),

$$\begin{aligned} \Delta v_{cv}^x(k_{cv}, \varphi, B_x) &\simeq \mp \frac{\sin 2\varphi}{2\hbar k_{cv}} h_x, \\ \Delta v_{cv}^x(k_{cv}, \varphi, B_y) &\simeq \mp \frac{\sin^2 \varphi}{\hbar k_{cv}} h_y. \end{aligned} \quad (\text{B9})$$

-
- * Electronic address: luhz@hku.hk
† Electronic address: sshen@hkucc.hku.hk
- ¹ D. D. Awschalom and M. E. Flatte, *Nat. Phys.* **3**, 153 (2007).
 - ² D. Awschalom, *Physics* **2**, 50 (2009).
 - ³ S. D. Ganichev, E. L. Ivchenko, V. V. Bel'kov, S. A. Tarasenko, M. Sollinger, D. Weiss, W. Wegscheider, and W. Prettl, *Nature* **417**, 153 (2002).
 - ⁴ S. D. Ganichev and W. Prettl, *Journal of Physics: Condensed Matter* **15**, R935 (2003).
 - ⁵ Y. Kato, R. C. Myers, A. C. Gossard, and D. D. Awschalom, *Science* **306**, 1910 (2004).
 - ⁶ J. Wunderlich, B. Kaestner, J. Sinova, and T. Jungwirth, *Phys. Rev. Lett.* **94**, 047204 (2005).
 - ⁷ X. W. He, B. Shen, Y. H. Chen, Q. Zhang, K. Han, C. M. Yin, N. Tang, F. J. Xu, C. G. Tang, Z. J. Yang, et al., *Phys. Rev. Lett.* **101**, 147402 (2008).
 - ⁸ J. Wunderlich, A. C. Irvine, J. Sinova, B. G. Park, L. P. Zarbo, X. L. Xu, B. Kaestner, V. Novak, and T. Jungwirth, *Nat. Phys.* **5**, 675 (2009).
 - ⁹ A. Haché, Y. Kostoulas, R. Atanasov, J. L. P. Hughes, J. E. Sipe, and H. M. van Driel, *Phys. Rev. Lett.* **78**, 306 (1997).
 - ¹⁰ R. D. R. Bhat and J. E. Sipe, *Phys. Rev. Lett.* **85**, 5432 (2000).
 - ¹¹ M. J. Stevens, A. L. Smirl, R. D. R. Bhat, A. Najmaie, J. E. Sipe, and H. M. van Driel, *Phys. Rev. Lett.* **90**, 136603 (2003).
 - ¹² J. Hübner, W. W. Rühle, M. Klude, D. Hommel, R. D. R. Bhat, J. E. Sipe, and H. M. van Driel, *Phys. Rev. Lett.* **90**, 216601 (2003).
 - ¹³ H. Zhao, E. J. Loren, H. M. van Driel, and A. L. Smirl, *Phys. Rev. Lett.* **96**, 246601 (2006).
 - ¹⁴ R. D. R. Bhat, F. Nastos, A. Najmaie, and J. E. Sipe, *Phys. Rev. Lett.* **94**, 096603 (2005).
 - ¹⁵ S. Tarasenko and E. Ivchenko, *JETP Lett.* **81**, 231 (2005).
 - ¹⁶ H. Zhao, X. Pan, A. L. Smirl, R. D. R. Bhat, A. Najmaie, J. E. Sipe, and H. M. van Driel, *Phys. Rev. B* **72**, 201302(R) (2005).
 - ¹⁷ X. D. Cui, S. Q. Shen, J. Li, Y. Ji, W. K. Ge, and F. C. Zhang, *Appl. Phys. Lett.* **90**, 242115 (2007).
 - ¹⁸ J. Li, X. Dai, S.-Q. Shen, and F. C. Zhang, *Appl. Phys. Lett.* **88**, 162105 (2006).
 - ¹⁹ B. Zhou and S.-Q. Shen, *Phys. Rev. B* **75**, 045339 (2007).
 - ²⁰ S. D. Ganichev, V. V. Bel'kov, S. A. Tarasenko, S. N. Danilov, S. Giglberger, C. Hoffmann, E. L. Ivchenko, D. Weiss, W. Wegscheider, C. Gerl, et al., *Nat. Phys.* **2**, 609 (2006).
 - ²¹ V. V. Bel'kov, S. D. Ganichev, E. L. Ivchenko, S. A. Tarasenko, W. Weber, S. Giglberger, M. Olteanu, H. Tranitz, S. N. Danilov, P. Schneider, et al., *J. Phys.: Condens. Matter* **17**, 3405 (2005).
 - ²² H. Diehl, V. A. Shalygin, S. N. Danilov, S. A. Tarasenko, V. V. Bel'kov, D. Schuh, W. Wegscheider, W. Prettl, and S. D. Ganichev, *J. Phys.: Condens. Matter* **19**, 436232 (2007).
 - ²³ J. Dai, H.-Z. Lu, C. L. Yang, S.-Q. Shen, F.-C. Zhang, and X. Cui, *Phys. Rev. Lett.* **104**, 246601 (2010).
 - ²⁴ S. D. Ganichev, V. V. Belkov, L. E. Golub, E. L. Ivchenko, P. Schneider, S. Giglberger, J. Eroms, J. D. Boeck, G. Borghs, W. Wegscheider, et al., *Phys. Rev. Lett.* **92**, 256601 (2004).
 - ²⁵ S. Giglberger, L. E. Golub, V. V. Bel'kov, S. N. Danilov, D. Schuh, C. Gerl, F. Rohlffing, J. Stahl, W. Wegscheider, D. Weiss, et al., *Phys. Rev. B* **75**, 035327 (2007).
 - ²⁶ P. Yu and M. Cardona, *Fundamentals of semiconductors* (Springer, 2001), 3rd ed.
 - ²⁷ F. Stern and W. E. Howard, *Phys. Rev.* **163**, 816 (1967).
 - ²⁸ A. A. Gorbatsevich, V. V. Kapaev, and Y. V. Kopaev, *JETP Lett.* **57**, 580 (1993).
 - ²⁹ S. A. Tarasenko, *Phys. Rev. B* **77**, 085328 (2008).
 - ³⁰ F. Nastos, J. Rioux, M. Strimas-Mackey, B. S. Mendoza, and J. E. Sipe, *Phys. Rev. B* **76**, 205113 (2007).
 - ³¹ R. Boyd, *Nonlinear optics* (Elsevier, 2008), 3rd ed.
 - ³² R. Winkler, *Spin-orbit Coupling Effects in Two-Dimensional Electron and Hole Systems* (Springer, 2003).
 - ³³ T. P. S. III and F. F. Fang, *Phys. Rev. B* **35**, 7729 (1987).
 - ³⁴ J. Nitta, T. Akazaki, and H. Takayanagi, *Phys. Rev. Lett.* **78**, 1335 (1997).
 - ³⁵ J. Wang, B.-F. Zhu, and R.-B. Liu, *Phys. Rev. Lett.* **100**, 086603 (2008).

³⁶ J. Wang, B.-F. Zhu, and R.-B. Liu, arXiv:1001.1053 (2010).

³⁷ M. Dresselhaus, G. Dresselhaus, and A. Jorio, *Group Theory Application to the Physics of Condensed Matter* (Springer-Verlag,

2008).